J Polym Res (2010) 17:109–118
DOI 10.1007/s10965-009-9296-5

ORIGINAL PAPER

Effects of halloysite nanotubes on kinetics and activation energy of non-isothermal crystallization of polypropylene

Mingliang Du · Baochun Guo · Jingjing Wan · Quliang Zou · Demin Jia

Received: 22 December 2008 / Accepted: 6 April 2009 / Published online: 22 April 2009

Abstract Halloysite nanotubes (HNTs), a kind of naturally occurring silicates possessing typical fibular structure, were introduced to fabricate polypropylene (PP)/HNTs nanocomposites. The non-isothermal crystallization behaviors were investigated by differential scanning calorimetry (DSC) method according to different treatments. The results suggest, with the inclusion of HNTs in PP matrix, the nanocomposites crystallize at higher temperature regime, which are correlated with the heterogeneous nucleating effects of HNTs during the crystallization process of PP. The kinetics studies of crystallization show that PP nanocomposites possess faster crystallization process and higher activation energy due to the nucleating effect and hindrance effect of HNTs to the motion of PP chains. The polarized light microscopy (PLM) observations further show that HNTs serve as nucleation sites and accelerate the crystallization process.

Keywords Crystallization · Halloysite nanotubes · Polypropylene · Activation energy

Introduction

Polymer nanocomposites with inorganics have been focused on during the past two decades. Numerous studies show that, with the incorporation of a certain amount of nanosized inorganics, the nanocomposites exhibit promising properties such as increased modulus, strength, thermal stability, etc [1–6]. The reinforcement of polypropylene (PP) is important for its relatively inferior mechanical and thermal properties. Halloysite nanotubes (HNTs) are a kind of natural occurring aluminosilicates with nanotubular structures [7–9]. Compared with other inorganics such as silica, montmorillonite, and kaolinite, the unique geometry and the siloxane surface characteristics with lower hydroxyl density render their good dispersion in polymer matrix. Typically, as shown in Fig. 1, HNTs possess dominantly nanotubular structure with inner diameter and outer diameter of 20-30 nm and 50-60 nm, respectively. Recently, HNTs have been introduced to fabricate polymer nanocomposites with promising mechanical properties [10–15].

It is well recognized that the crystallinity and morphology are quite crucial to the mechanical performance of crystalline and semi-crystalline polymers [16, 17]. Consequently, understanding the crystallization behavior of PP nanocomposites is necessary to controlling the performance of the nanocomposites. Generally, the nanosized inclusions tend to facilitate the crystallization process of PP due to the heterogeneous nucleation. For instances, Bhattacharyya *et al*. [18] studied the effects of single wall carbon nanotube (SWCNT) on the crystallization behavior of PP and found that, though SWCNT dispersed poorly in PP matrix, the SWCNT aggregates or ropes act as nucleating sites for PP crystallization. Maiti *et al*. [19] studied the influence of crystallization on the morphology and mechanical properties of PP/clay nanocomposites and found the fine structure, morphology, and mechanical properties of PP/clay nanocomposites can be controlled by the intercalation through crystallizing at a suitable temperature. Zhang *et al*. [20] studied the influence of modified calcium carbonate on the

M. Du
Faculty of Materials and Textiles, Zhejiang Sci-Tech University, Hangzhou 310018, China

M. Du · B. Guo (✉) · J. Wan · Q. Zou · D. Jia
Department of Polymer Materials and Engineering, South China University of Technology, Guangzhou 510640, China
e-mail: psbcguo@scut.edu.cn

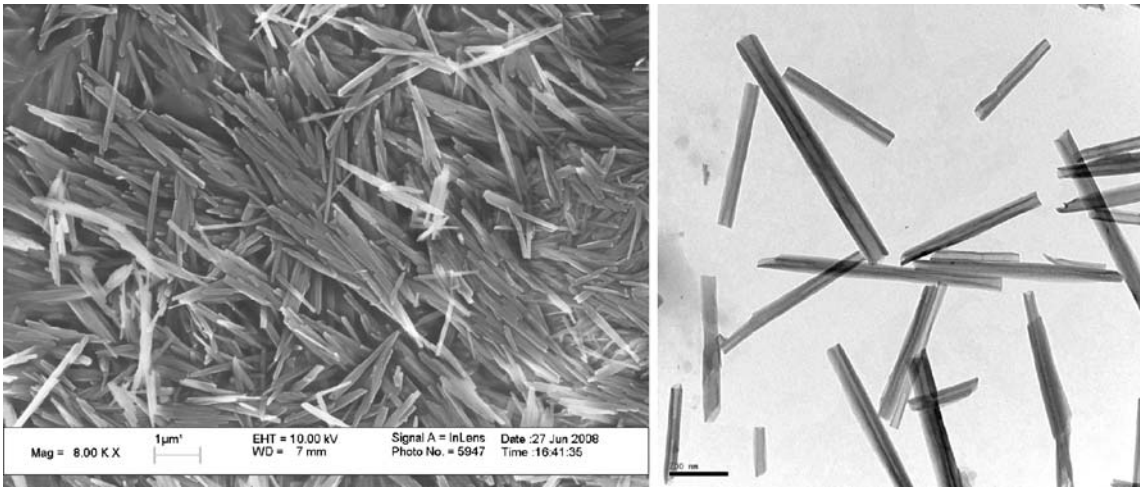

Fig. 1 Morphology of HNTs (left: SEM photo; right: TEM photo)

crystallization of PP. The results suggested that the particles of calcium carbonate decreased the spherulite growth rate and induced formation of β-form crystal of PP, and the impact strength of the composite was increased significantly. As reported by George *et al*. [21], the isothermal crystallization rate was increased with the addition of fumed silica to PP matrix and the presence of fumed silica was found to alter the effective energy barrier of crystallization.

Ning *et al*. [22] introduced HNTs to PP to prepare composites and studied the crystallization behavior of the composites, showing that HNTs serve as a nucleation agent and facilitate the crystallization of PP. However, the crystallization kinetics of PP/HNTs nanocomposites and the evaluation of physically meaningful parameters of the crystallization haven't been addressed. The present work attempts to study the non-isothermal crystallization kinetics of PP/HNTs nanocomposites. Such empirical kinetics equations as Avrami equation and Mo equation are used for the analysis of the dependences of crystallization rate and temperature of the nanocomposites on the HNTs content and cooling rate. In addition, Hoffman-Lauritzen theory is employed to evaluate the chain folding activation energy during the non-isothermal crystallization. The crystallization behavior of the nanocomposites is correlated to the nucleation and hindrance effects of HNTs on PP crystallization.

Experimental

Materials

Polypropylene (PP) granules were products of Guangzhou Petrochemical Co. Ltd. The melt flow index was determined as 2.84 g/10min (after ISO-1133: 1997(E)).

Halloysite nanotues (HNTs) were mined from Hubei Province, China. The HNTs were purified as follows: The HNTs were dissolved in water (10 wt-%) and then the sediment was removed. The water in the HNTs solution was removed through a centrifugation process. The purified HNTs were ground into 80 meshes fine powder. The Brunauer-Emmett-Teller (BET) specific surface area was determined as 50.45 m^2/g with a specific surface area and porosity analyzer, ASAP 2020 of Micromeritics.

Preparation of PP/HNTs nanocomposites

PP/HNTs nanocomposites were prepared with a twin-screw extruder and HNTs were utilized without any surface modification. The temperatures setting from the hopper to the die were 180/200/200/200/200/200°C, respectively. The screw speed was 100 rpm, and the pelletized granules were dried for 5 hours under 80°C.

Characterizations

Differential Scanning Calorimetry (DSC) DSC data was measured by NETZSCH DSC204 F1 using nitrogen as purging gas. To determine the non-isothermal crystallization behavior of PP and PP nanocomposites, the samples were heated to 200°C at ramping rate of 20°C/min, then the samples were kept at 200°C for 5 min to eliminate the thermal history before they were cooled down to 40°C at rate of 5°C, 10°C, 15°C, 20°C/min, respectively. The exothermic flows were recorded as a function of temperature.

To determine the equilibrium melting point of the samples, isothermal crystallization was also performed. The samples were heated to 200°C at ramping rate of 20°C/min and kept at 200°C for 5 min to eliminate the thermal history. Then the samples were quenched to the

crystallization temperature and kept for at least 30 min and then reheated to 200°C at ramping rate of 20°C/min. The endothermic and exothermic flows were recorded as a function of time.

The crystallinity was calculated based on the endothermic enthalpy (ΔH_f) as follows:

$$Crystallinity(\%) = \frac{\Delta H_f}{\Delta H_f^0 \times C}$$

Where ΔH_f and ΔH_f^o are the endothermic enthalpies of the sample and the PP with crystallinity of 100%, respectively. C is the PP weight percentage in the composite. The value of ΔH_f^o is 209 J/g according to the literature [23].

Scanning Electron Microscopy (SEM) The HNTs powder was plated with a thin layer of gold before the observations. The SEM observations were then performed using a LEO1530 VP SEM machine.

Transmission Electron Microscopy (TEM) The HNTs powder was dissolved in de-ion water at extremely diluted solution of about 0.5 wt-% and ultrasonified for about 2 hours. The HNTs solution was dropped onto the surface of the copper mesh coated with carbon film, dried for 1 hour at 80°C and then used for TEM observation. The TEM observations were done using a Philip CM12 electron transmission microscope machine at an accelerating voltage of 30 kV.

Polarized Light Microscopy (PLM) Morphologies of the crystallites of PP and PP nanocomposites were observed with an Olympus BX51 polarized light microscopy. The samples were heated to 200°C and kept for 3 min to eliminate the thermal history, and then jumped to 130°C for the PLM observation.

Results and disscussion

Theoretical background for non-isothermal crystallization kinetics

As well recognized, Avrami equation can be used to simulate the isothermal and non-isothermal crystallization of polymer. So far, many methods, such as Jeziorny method [24], Ozawa method [25], and Mo method [26], have been developed to revise Avrami equation. Avrami equation could be expressed as follows:

$$\ln[-\ln(1-Xt)] = \ln(K) + n \cdot \ln t \quad (1)$$

Where X_t is the crystallinity at crystallization time t, K and n are Avrami crystallization constant and Avrami exponent, respectively. ln(K) and n can be obtained by the linear fit of ln[–ln(1–Xt)] versus ln$t$. In this expression, t equals to $(T_0\text{-}T)/\Phi$, where T_0 is initial crystallization temperature, T is crystallization temperature, Φ is the cooling rate. In Jeziorny method, to eliminate the effect of cooling rate, the following expression is used to calibrate the Avrami crystallization constant K:

$$\lg Kc = \frac{\lg K}{\Phi} \quad (2)$$

Where Kc is Jeziorny crystallization constant.

In Ozawa method, the non-isothermal crystallization is regarded as being composed of numerous infinitesimal isothermal crystallizations. Consequently, a factor ϕ is introduced to Avrami equation:

$$X_t = 1 - \exp(-K(T)/\phi^m) \quad (3)$$

Where $K(T)$ is dynamic parameter, m is Ozawa coefficient, which is related to the growth of the crystalline process.

Mo combined Avrami equation and Ozawa equation and proposed a new mathematic treatment for non-isothermal crystallization behavior of polymers:

$$\ln\phi = \ln F(T) - a\ln t \quad (4)$$

Where $F(T) = [K(T)/Z_t]^{1/m}$, a = n/m, n is Avrami exponent, m is Ozawa factor. $F(T)$ is the cooling rate that should be reached to achieve a certain crystallinity in a certain time. $F(T)$ and a can be obtained from the intercept and slope of the linear fit of ln ϕ versus ln t.

In addition, the activation energy of non-isothermal crystallization can be obtained from Kissinger equation [27]:

$$\frac{d[\ln(\phi/T_p^2)]}{d(1/T_p)} = -\frac{\Delta E_d}{R} \quad (5)$$

Where R is gas constant, ΔE_d is activation energy of crystallization, T_p is peak temperature of crystallization. ΔE_d is obtained from the slope of the linear curves of $\ln(\phi/T_p^2)$ versus $1/T_p$. However, as demonstrated by Vyazovin *et al*. [28], the above Kissinger method usually provides unacceptable values of activation energy (E) because it can only evaluate the overall rate and activation energy of the non-isothermal crystallization. The Kissinger method is only applicable to single-step processes whose kinetics can be adequately represented by a single value of E. Recently, the isoconversional method has been applied to eliminate the above problems and the physically meaningful parameters for the crystallization could be evaluated on the base of Hoffman-Lauritzen [29] theory. According to Hoffman-Lauritzen theory, a dependence of the linear

growth rate of polymer crystal, G, depends on the temperature and can be described as follows:

$$G = G_0 \exp\left(\frac{-U^*}{R(T - T_\infty)}\right) \exp\left(\frac{-K_g}{T\Delta Tf}\right) \quad (6)$$

Where G_0 is the pre-exponential factor, U^* is the activation energy of the segmental jump, $\Delta T = T_m^0 - T$ is the under-cooling, $f = 2T/(T_m^0 + T)$ is the correction factor, T_∞ is a hypothetical temperature at which viscous flow ceases and is usually [29] taken 30 K below the glass transition temperature (T_g, in the present work T_∞ takes 253.15 K for neat PP and their composites). The kinetic parameter K_g has the following form:

$$K_g = \frac{nb\sigma\sigma_e T_m^0}{\Delta h_f^0 k_B} \quad (7)$$

Where n takes the value of 4 in the present work, b is the distance between two adjacent fold planes (for PP $b = 6.56 \times 10^{-10}$ m), σ and σ_e are the lateral and folding surface free energy, respectively ($\sigma = 8.79 \times 10^{-3}$ J/m^2), T_m^0 is the equilibrium melting temperature, Δh_f^0 is the heat of fusion per unit volume of crystal (1.34×1.08 J/m^3), k_B is the Boltzmann constant [30]. The parameters U^* and K_g are usually determined by measuring microscopically the growth rate in a series of non-isothermal runs and substituting the measured value in rearranged Eq. (6):

$$\ln G + \frac{U^*}{R(T - T\infty)} = \ln G_0 - \frac{K_g}{T\Delta Tf} \quad (8)$$

And in narrow temperature region, an explicit dependence of effective activation energy (E) on T can be derived from Eq. 6 as follows [28]:

$$E_\alpha(T) = -R\frac{d\ln G}{dT^{-1}} = U^*\frac{T^2}{(T - T_\infty)^2} + K_g R \times \frac{(T_m^0)^2 - T^2 - T_m^0 T}{\Delta T^2 T} \quad (9)$$

E_α represents the effective activation energy when the crystallinity degree is α. According to theory of Hoffman-Weeks [31], the equilibrium melting temperature (T_m^0) can

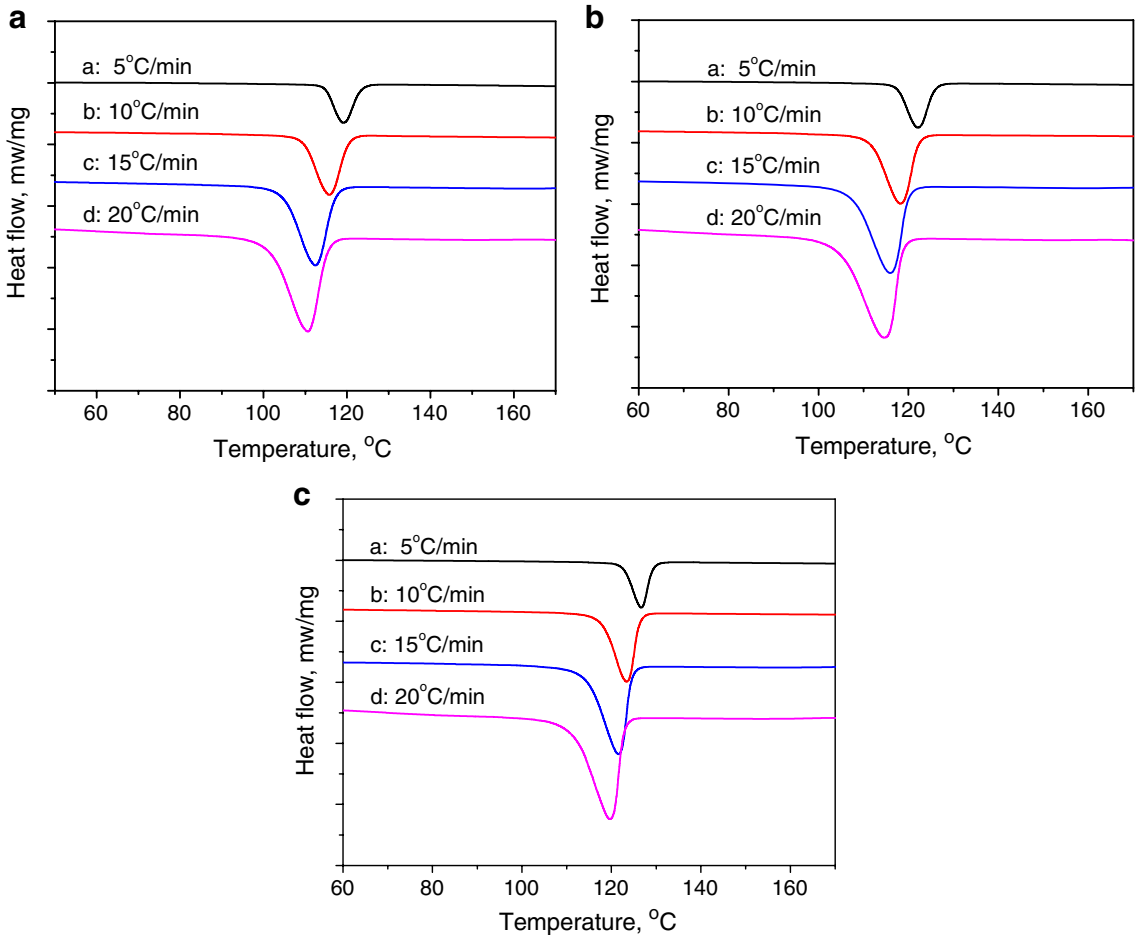

Fig. 2 Non-isothermal crystallization curves of PP and PP nanocomposites a) PP; b) PP/HNTs (100/5); c) PP/HNTs (100/30)

Table 1 Non-isothermal crystallization parameters of PP and PP nanocomposites calculated by the Jeziorny method

Samples	Φ, °C/min	n	logKc	$t_{1/2}$, min	T_p, °C
Neat PP	5	4.15	0.363	1.20	119.2
	10	5.92	0.602	0.750	115.6
	15	8.18	0.690	0.603	112.4
	20	8.96	0.796	0.525	110.7
PP/HNTs (100/5)	5	4.85	0.326	1.20	122.1
	10	7.05	0.550	0.800	118.2
	15	9.00	0.694	0.610	116.0
	20	11.5	0.803	0.580	114.4
PP/HNTs (100/30)	5	6.50	0.203	1.10	126.6
	10	9.15	0.466	0.650	123.3
	15	11.8	0.640	0.567	121.3
	20	13.9	0.764	0.458	119.6

be obtained by linear extrapolation of T_m versus T_c data to intersect the line T_m=T_c and the intersection point is the $T_m{}^0$.

Based on the nonlinear isoconversional method [32], the effective activation energy for the non-isothermal crystallization is calculated in accordance with the Eq 10 and the specific derivation process can be figured out by according to references [33, 34].

$$\Omega(E_\alpha) = \min\left|\sum_{i=1}^{n}\sum_{j\neq i}^{n}\frac{\varphi_j \bullet I(E_\alpha, T_{\alpha,i})}{\varphi_i \bullet I(E_\alpha, T_{\alpha,j})} - n(n-1)\right| \qquad (10)$$

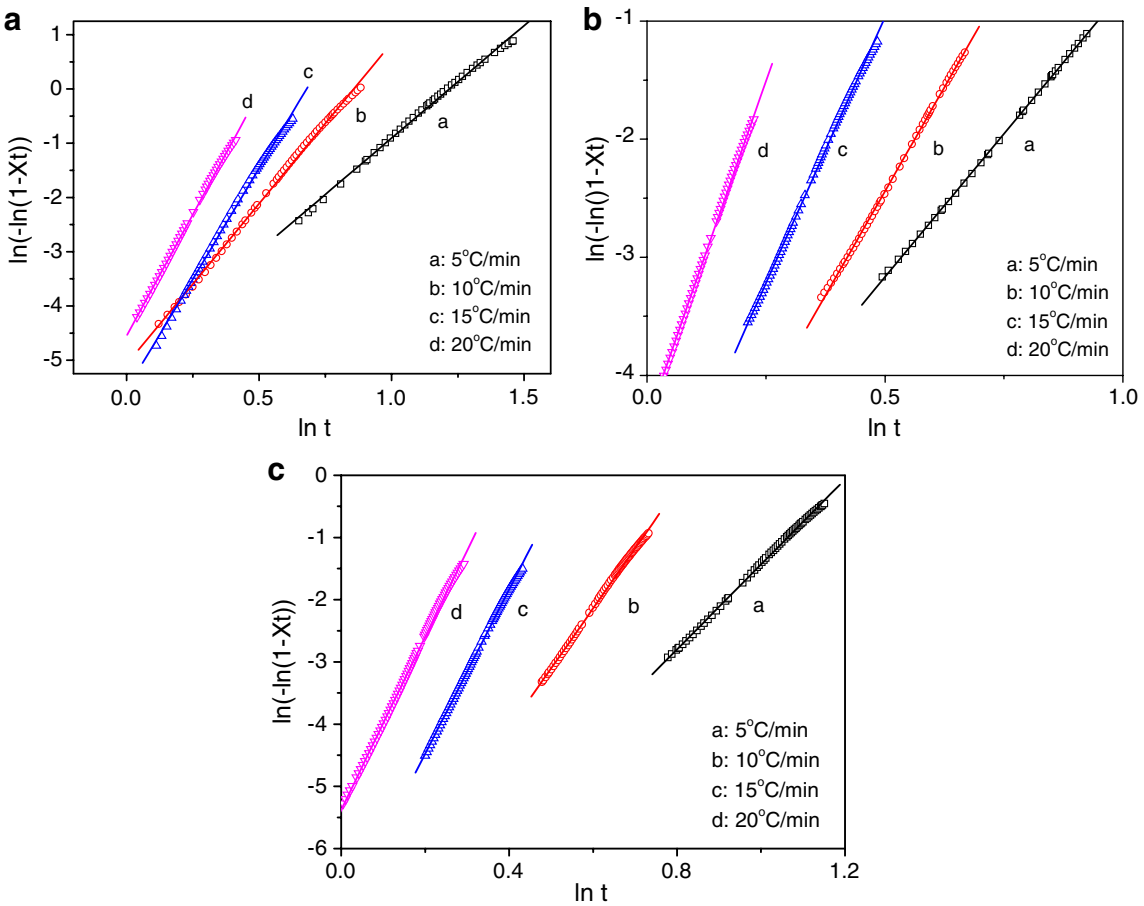

Fig. 3 Non-isothermal crystallization curves of PP and PP nanocomposites processed by the Jeziorny method a) PP; b) PP/HNTs (100/5); c) PP/HNTs (100/30)

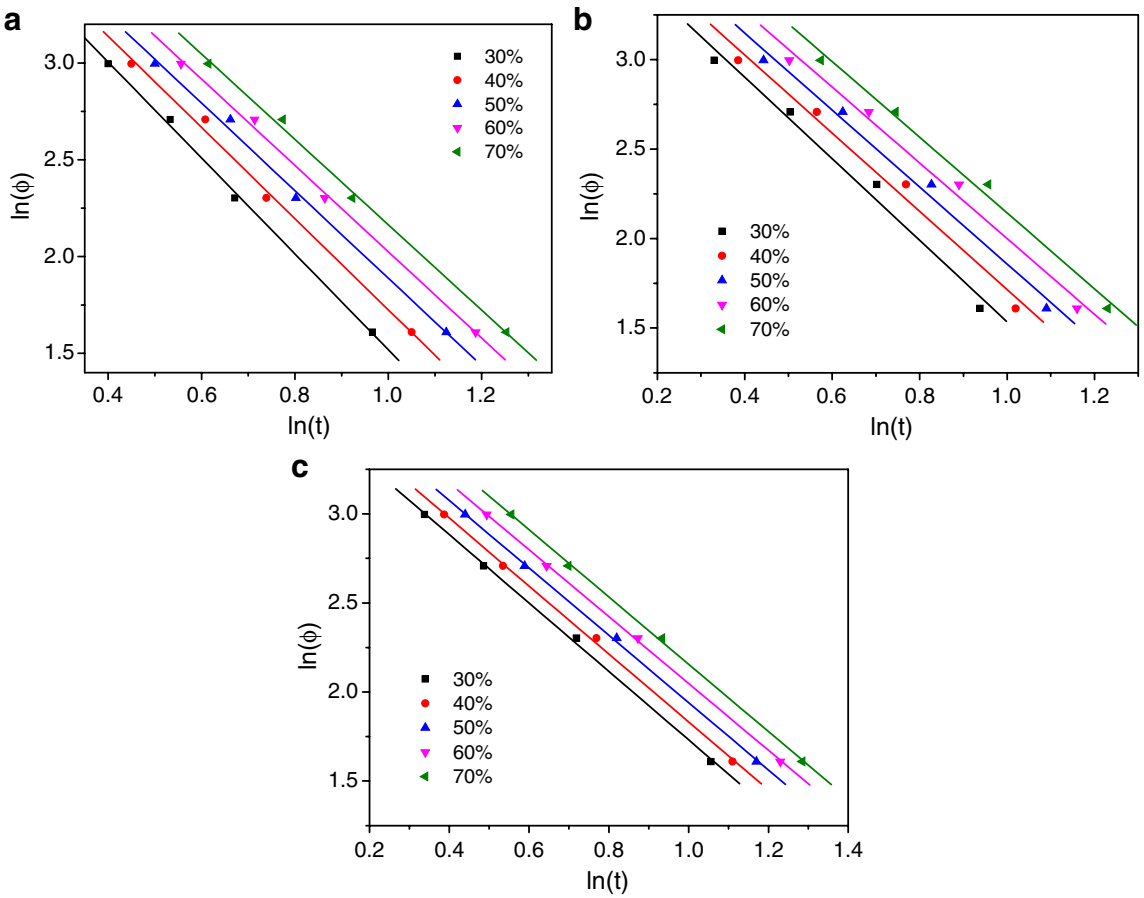

Fig. 4 Non-isothermal crystallization curves of PP and PP nanocomposites processed by the Mo method a) PP; b) PP/HNTs (100/5); c) PP/HNTs (100/30)

Table 2 Non-isothermal crystallization parameters of PP and PP nanocomposites calculated by the Mo method

Samples	X_t, %	ln($F(T)$)	a
Neat PP	30	3.90	2.48
	40	4.08	2.36
	50	4.15	2.26
	60	4.25	2.23
	70	4.37	2.21
PP/HNTs (100/5)	30	3.81	2.28
	40	3.90	2.18
	50	4.00	2.15
	60	4.11	2.11
	70	4.26	2.11
PP/HNTs (100/30)	30	3.65	1.92
	40	3.74	1.90
	50	3.83	1.89
	60	3.92	1.88
	70	4.04	1.89

Here

$$I(E_\alpha, T_\alpha) = \int_{T_0}^{T_\alpha} \exp\left(\frac{-E_\alpha}{RT_\alpha}\right) dT \tag{11}$$

This integral is determined with the help of a Doyle's approximation [35]

$$I(E_\alpha, T_\alpha) \cong \frac{E_\alpha}{R} \exp\left(-5.331 - 1.052\frac{E_\alpha}{RT_\alpha}\right) \tag{12}$$

And φ stands for the cooling rate; n represents the number of cooling rates, in the present study is 5. By substituting a series of different φ_i, $T_{\alpha,i}$, (i = 1, 2, … , n) estimated at the same α on the DSC curves into the Eq. 10, we can obtain the minimum value of E_α.

Non-isothermal crystallization kinetics of PP/HNTs nanocomposites

To evaluate the effects of HNTs on the non-isothermal crystallization behavior of PP, the exothermic curves of the

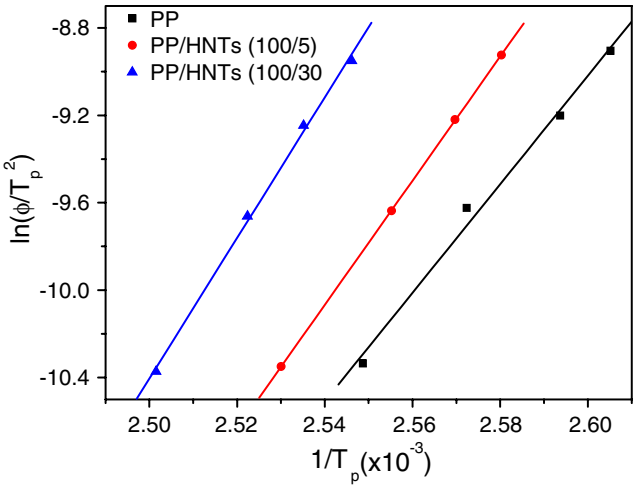

Fig. 5 Curves of $\ln(\phi/T_p^2)$ versus $1/T_p$ for PP and PP nanocomposites

samples at various cooling rates are presented in Fig. 2. The peak temperatures (T_p) of crystallization of PP and the PP/HNTs nanocomposites are summarized in Table 1. From Table 1, it can be observed that the T_p of PP/HNTs nanocomposites increases with respect to PP. In addition, more HNTs incorporated, much higher T_p are obtained. It is believed that the well dispersed HNTs serve as heterogeneous nucleating agent and thus facilitate the crystallization process.

The non-isothermal crystallization behavior was then processed via Jeziorny method and the results were shown in Fig. 3 and Table 1. From Fig. 3, it can be observed that the non-isothermal crystallization curves of PP and PP composites obtained via Jeziorny method possess good linearity, indicating the suitability of Jeziorny method in the treatment of non-isothermal crystallization of PP and PP nanocomposites. It is believed that Avrami exponent is related to the nucleation mechanism and growth mechanism of PP and usually is about from 1 to 3. However, the crystallization of polymer composites is a very complicated process, which is much more complicated than Avrami equation and other mathematical models; consequently, the value of actual Avrami exponent of the crystallization is quite higher than the theoretical values. It also can be seen that the Avrami exponent of the nanocomposites increases with HNTs loading, which is ascribed to the effects of HNTs on the nucleation and growth of the crystals of PP. With the introduction of HNTs, PP crystallizes at higher temperature and the $t_{1/2}$ is decreased to some extent, which are attributed to the promoted nucleation and crystallization of PP by HNTs.

Non-isothermal crystallization curves of PP and PP nanocomposites processed by the Mo method and the crystallization parameters of PP and PP nanocomposites calculated by the Mo method are shown in Fig. 4 and Table 2, respectively. In Mo treatment method, *F(T)* means the cooling rate that should be taken to obtain the crystallinity in a certain time. From Table 2, it can be observed that the value of *F(T)* increases with the increase of crystallinity. However, at the same crystallinity, the value of *F(T)* for PP nanocomposites is lower than that for neat PP, suggesting that, to obtain the same crystallinity, lower cooling rate should be taken for PP nanocomposites than that of neat PP, which is also an indication of promoted crystallization of PP by HNTs.

Activation energy of non-isothermal crystallization of PP/HNTs nanocomposites

Figure 5 shows the curves of $\ln(\phi/T_p^2)$ versus $1/T_p$ for PP and PP nanocomposites via Kissinger method. The activation energies obtained from Kissinger method are listed in Table 3. As shown in Table 3, the calculated activation energy increases with the incorporation of HNTs in PP matrix, which may result from the confinement effect of HNTs on the motion of PP chains. The similar confinement effects were also found in PP/montmorillonite nanocomposites [36, 37]. Consequently, both the nucleation effect and confinement effect influence the crystallization of PP and PP nanocomposites. The former promotes the crystallization of PP, however, the latter is unfavorable for the crystallization of PP. It is mentioned above that the presence of HNTs leads to faster nucleation. The inclusion of HNTs however confines the growth of the crystallites as indicated by the higher activation energy. In the present systems, the former factor dominates, resulting in faster overall crystallization and shorter $t_{1/2}$.

As discussed previously, according to the Hoffman-Weeks theory, T_m^0 can be obtained by linear extrapolation of T_m versus T_c data to intersect the line T_m=T_c and the

Table 3 Crystallization activation energies of PP and PP nanocomposites

Samples	PP	PP/HNTs nanocomposites (100/5)	PP/HNTs nanocomposites (100/30)
Activation energy, KJ/mol	-206.2	-236.1	-267.3

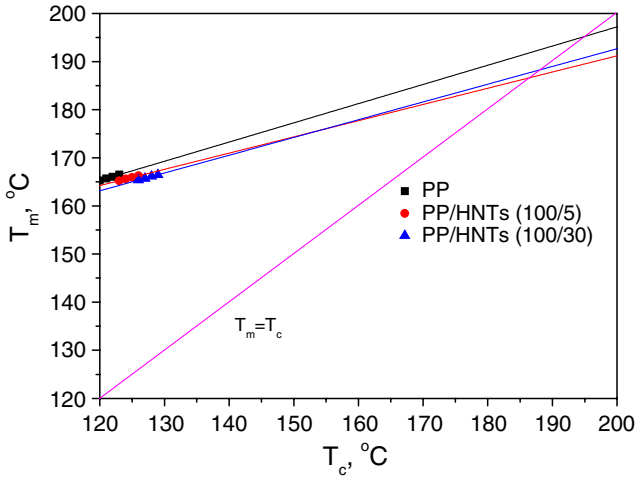

Fig. 6 Melting temperature as a function of crystallization temperature for PP and its nanocomposites

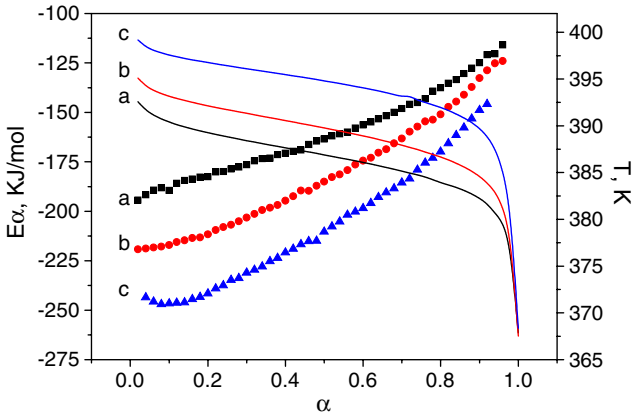

Fig. 7 Dependence of the effective activation energy on the relative extent of crystallization and the variation of the average temperature with the relative extent of crystallization (solid lines) (**a** neat PP, **b** PP/HNTs (100/5), **b** PP/HNTs (100/30))

intersection point is the T_m^0. In the present study, the T_m^0 of PP and PP nanocomposites are shown in Fig. 6 and listed in Table 4. Figure 7 shows the dependence of the effective activation energy on the relative extent of crystallization and the variation of the average temperature with the relative extent of crystallization obtained from the isoconversional method. From Fig. 7, it can be seen that at the same crystallinity, the absolute value of E_α of PP/HNTs nanocomposites is always higher than that of neat PP, and higher HNTs content in PP matrix further improves the absolute value of E_α of the nanocomposite. In addition, it can be seen that, with the increase of crystallinity, all the absolute values of E_α of PP and PP/HNTs nanocomposite decrease.

In addition, the E_a -T curves were plotted to obtain the values of U^* and K_g by fitting the Eq. 9 with Origin7.0 software and the results are summarized in Fig. 8 and Table 4. The R^2 represent the dependency of the fitting curves and the data, the value of which is very close to 1 indicating the well fitting. As shown in the table, the values of σ_e for the composites are higher than that for neat PP, indicating higher folding surface energy of PP chains, which is consistent with the results of E and E_a obtained from Kissinger method and isoconversional method.

To further evaluate the nucleation effects of HNTs on crystallization of PP, the evolutions of sperulites of PP and PP nanocomposites were observed via polarized light microscopy (PLM) under isothermal condition. Figure 9 shows the PLM photos of PP and PP/HNTs nanocomposites crystallized at 130°C. From the photos it can be seen that with the incorporation of HNTs in PP matrix, much more growing sites for the spherulites occur and, with the evolution of crystallization process, the growth of the spherulite is confined by the surrounding spherulites.

Table 4 Kinetic data for no-isothermally crystallized of neat PP and its nanocomposites

Sample	Neat PP	PP/HNTs(100/5)	PP/HNTs(100/30)
U^*(J/mol)	9748.04	14532.75	22271.50
$K_g(10^5K^2)$	6.698	7.526	8.017
R^2	0.99789	0.99824	0.99745
T^o_m(K)	468.0	459.3	461.1
$\sigma\sigma_e(10^{-3}J^2/m^4)$	1.01	1.15	1.23
$\sigma_e(10^{-3}J/m^2)$	0.1147	0.1314	0.1394

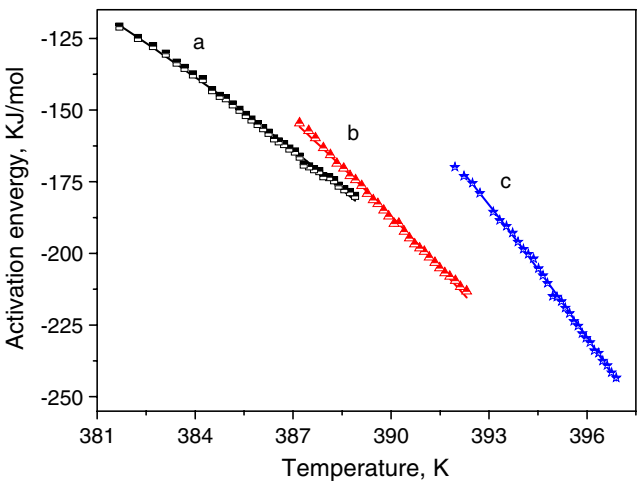

Fig. 8 Dependence of the effective activation energy on average temperature and their fits of Equation (solid lines) (**a** neat PP, **b** PP/HNTs (100/5), **b** PP/HNTs (100/30))

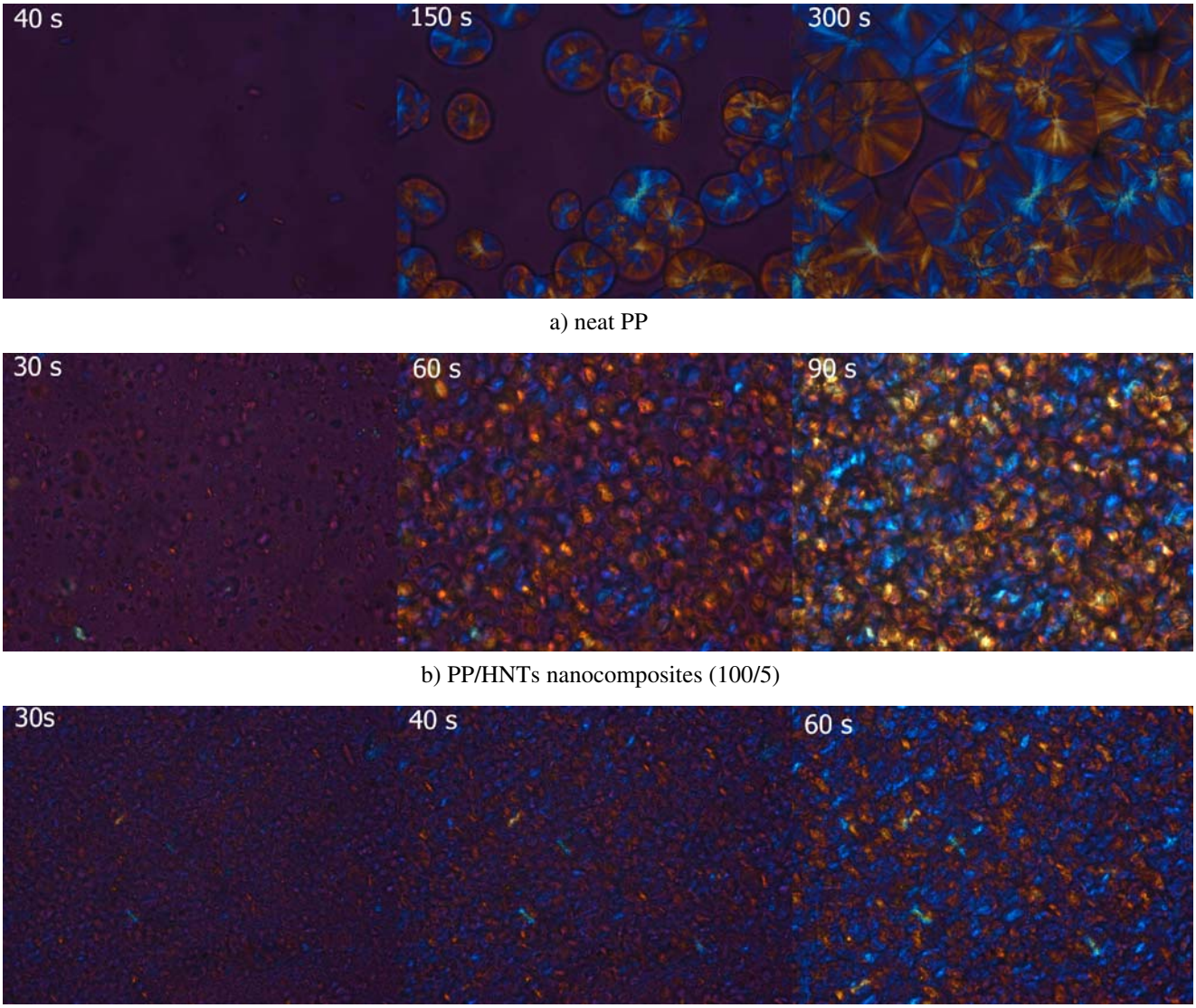

Fig. 9 Evolution of spherulites of PP and PP nanocomposites at 130°C (500×)

Consequently, the size of spherulites becomes much smaller, and more HNTs added, smaller spherulites are observed.

Conclusions

HNTs were introduced to prepare PP/HNTs nanocomposites. The non-isothermal crystallization behaviors were investigated by DSC method according to different treatments. The results suggested, with the inclusion of HNTs in PP matrix, the nanocomposites crystallized at higher temperature regime, which were correlated with the heterogeneous nucleating effect of HNTs during the crystallization process of PP. The kinetic studies of crystallization showed that PP nanocomposites possessed faster crystallization process and higher activation energy due to the nucleating effect and hindrance effect of HNTs to the motion of PP chains, respectively. The polarized light microscopy (PLM) observation further showed that HNTs served as nucleation sites and accelerated the crystallization process.

Acknowledgements We are grateful to the financial support by the project of National Natural Science Foundation of China (NSFC) (Grant numbers: 50603005, 50873035), Postdoctoral Science Foundation of China (Grant number: 20080430111), and Postdoctoral Foundation of South China University of Technology (Grant number: 20080207).

References

1. Ray SS, Okamoto M (2003) Prog Polym Sci 28(11):1539–1641. doi:10.1016/j.progpolymsci.2003.08.002
2. Gilman JW (1999) Appl Clay Sci 15(1-2):31–49. doi:10.1016/S0169-1317(99)00019-8
3. Kawasumi M, Hasegawa N, Kato M, Usuki A, Okada A (1997) Macromolules 30(20):6333–6338. doi:10.1021/ma961786h
4. Chan CM, Wu JS, Li JX, Cheung YK (2002) Polymer (Guildf) 43 (10):2981–2992. doi:10.1016/S0032-3861(02)00120-9
5. Moniruzzaman M, Winey KI (2006) Macromolecules 39 (16):5194–5205. doi:10.1021/ma060733p
6. Ji XL, Hampsey JE, Hu QY, He JB, Yang ZZ, Lu YF (2003) Chem Mater 15(19):3656–3662. doi:10.1021/cm0300866
7. Joussein E, Petit S, Churchman J, Theng B, Righi D, Delvaux B (2005) Clay Miner 40(4):383–426. doi:10.1180/0009855054040180
8. Brindley GW, Brown G (1980) Crystal Structures of Clay Minerals and their X-ray Identification. Mineralogical Society, London, pp 1–123
9. Bailey SW (1988) Reviews in Mineralogy, Bailey SW. Mineralogical Society of America, Chelsea, MI, pp 675–725
10. Liu MX, Guo BC, Zou QL, Du ML, Jia DM (2008) Nanotechnology 19(20):205709. doi:10.1088/0957-4484/19/20/205709
11. Liu MX, Guo BC, Du ML, Cai XJ, Jia DM (2007) Nanotechnology 18(45):455703. doi:10.1088/0957-4484/18/45/455703
12. Du ML, Guo BC, Liu MX, Jia DM (2007) Polym Polym Compos 15(4):321–328
13. Du ML, Guo BC, Liu MX, Jia DM (2006) Polym J 38(11):1198–1204. doi:10.1295/polymj.PJ2006038
14. Du ML, Guo BC, Jia DM (2006) Eur Polym J 42(6):1362–1369. doi:10.1016/j.eurpolymj.2005.12.006
15. Du ML, Guo BC, Cai XJ, Jia ZX, Liu MX, Jia DM (2008) E-polym 18:1–14
16. Bureau MN, Denault J, Cole KC, Bureau MN, Denault J, Cole KC, Enright GD (2002) Polym. Eng Sci 42(9):1897–1906
17. Rao YQ, Greener J, Avila-Orta CA, Hsiao BS, Blanton TN (2008) Polymer (Guildf) 49(10):2507–2514. doi:10.1016/j.polymer.2008.03.046
18. Bhattacharyya AR, Sreekumar TV, Liu T, Kumar S, Ericson LM, Hauge RH, Smalley RE (2003) Polymer (Guildf) 44(8):2373–2377. doi:10.1016/S0032-3861(03)00073-9
19. Maiti P, Nam PH, Okamoto M, Hasegawa N, Usuki A (2002) Macromoluecules 35(6):2042–2049. doi:10.1021/ma010852z
20. Zhang QX, Yu ZZ, Xie XL, Mai YW (2004) Polymer (Guildf) 45 (17):5985–5994. doi:10.1016/j.polymer.2004.06.044
21. Papageorgiou GZ, Achilias DS, Bikiaris DN, Bikiaris DN, Karayannidis GP (2005) Thermochim Acta 42(1-2):117–128. doi:10.1016/j.tca.2004.09.001
22. Ning NY, Yin QJ, Luo F, Zhang Q, Du R, Fu Q (2007) Polymer (Guildf) 48(25):7374–7384. doi:10.1016/j.polymer.2007.10.005
23. Brandrup J, Immergut EH (1989) Polymer Handbook, 3rd edn. Chapter V. Wiley, New York
24. Jeziorny A (1978) Polymer (Guildf) 19:1142–1148. doi:10.1016/0032-3861(78)90060-5
25. Ozawa T (1971) Polymer (Guildf) 12(3):150–158. doi:10.1016/0032-3861(71)90041-3
26. Yin JH, Mo ZX (2001) Modern Polymer Physics. Science Press, Beijing
27. Kissinger HE (1956) J Res Natl Stan 57:17–21
28. Vyazovkin S, Sbirrazzuoli N (2004) Macromol Rapid Commun 25 (6):733–738. doi:10.1002/marc.200300295
29. Hoffman JD, Davis GT, Lauritzen JI in: Treatise on Solid State Chemistry, NB Hannay Ed, Plenum, New York 1976, Vol. 3, p. 497
30. Xiao WC, Wu PY, Feng JC (2008) J Appl Polym Sci 108:3370–3379. doi:10.1002/app.27997
31. Marand H, Xu JN, Srinivas S (2008) Macromolecules 31 (23):8219–8229. doi:10.1021/ma980747y
32. Vyazovkin S, Dollimore D (1996) J Chem Inf Comput Sci 36:42–45. doi:10.1021/ci950062m
33. Vyazovkin S (1997) J Comput Chem 18:393–402. doi:10.1002/(SICI)1096-987X(199702)18:3<393::AID-JCC9>3.0.CO;2-P
34. Vyazovkin S (2001) J Comput Chem 22:178–183. doi:10.1002/1096-987X(20010130)22:2<178::AID-JCC5>3.0.CO;2-#
35. Doyle CD (1962) J Appl Polym Sci 6:639–642. doi:10.1002/app.1962.070062406
36. Li J, Zhou CX, Gang W (2003) Polym Test 22(2):217–223. doi:10.1016/S0142-9418(02)00085-5
37. Solomon MJ, Almusallam AS, Seefeldt KF, Somwangthanaroj A, Varadan P (2001) Macromolecules 34(6):1864–1872. doi:10.1021/ma001122e